

# Engineering DNA nanotubes for resilience in an *E. coli* TXTL system

Melissa A. Klocke<sup>1,†</sup>, Jonathan Garamella<sup>2,†</sup>, Hari K. K. Subramanian<sup>1</sup>, Vincent Noireaux<sup>2,\*</sup>, and Elisa Franco<sup>1,\*</sup>

<sup>1</sup>Mechanical Engineering, University of California, Riverside, Riverside, CA, USA and <sup>2</sup>School of Physics and Astronomy, University of Minnesota, Minneapolis, MN, USA

\*Corresponding authors: E-mails: efranco@engr.ucr.edu; andnoireaux@umn.edu

<sup>†</sup>These authors contributed equally to this work.

## Abstract

Deoxyribonucleic acid (DNA) nanotechnology is a growing field with potential intracellular applications. In this work, we use an *Escherichia coli* cell-free transcription–translation (TXTL) system to assay the robustness of DNA nanotubes in a cytoplasmic environment. TXTL recapitulates physiological conditions as well as strong linear DNA degradation through the RecBCD complex, the major exonuclease in *E. coli*. We demonstrate that chemical modifications of the tiles making up DNA nanotubes extend their viability in TXTL for more than 24 h, with phosphorothioation of the sticky end backbone being the most effective. Furthermore, we show that a Chi-site double-stranded DNA, an inhibitor of the RecBCD complex, extends DNA nanotube lifetime significantly. These complementary approaches are a first step toward a systematic prototyping of DNA nanostructures in active cell-free cytoplasmic environments and expand the scope of TXTL utilization for bioengineering.

**Key words:** DNA nanostructure; *in vitro* systems; cell-free systems; DNA nuclease; synthetic biology.

## 1. Introduction

Several attempts to transition deoxyribonucleic acid (DNA) nanotechnology from ideal test tube conditions to living systems have been carried out in recent years (1). Interfacing DNA nanostructures with biology, however, faces many challenges, a major one being conferring resilience to the nanostructures for *in vivo* operation. In this work, we engineered synthetic DNA nanostructures and developed methods to increase their lifetime in an all *Escherichia coli* cell-free transcription–translation (TXTL) system. TXTL, used as an active cytoplasmic environment (2, 3), recapitulates the physiological conditions found in cells (Figure 1b), as well as harsh linear DNA degradation through the RecBCD complex.

Synthetic DNA can be designed to fold into unique nano-scale structures, which can perform specific tasks, such as

drug delivery, intracellular scaffolding and synthetic-cell design (4–7). The diversity of DNA nanostructures, reported in the literature, illustrates the benefits of working with this versatile self-assembling material. Synthetic-DNA nanotubes assemble from DNA tiles via programmed interactions of the tile sticky ends (8, 9). Their geometry and mechanical properties are close to those of actin filaments and microtubules, suggesting that these nanotubes could serve as an artificial cytoskeleton in synthetic cells (8). They could operate as scaffolds to localize components, actively transport material and influence cell morphology. Further, DNA nanotubes tagged with fluorophores are easily observed with epifluorescence microscopy (Figure 1a), making characterization easier than for other nanometer-scale DNA structures.

Despite reports of DNA nanostructure stability in cell lysate and serum (10), we found that these nanotubes degrade within

**Submitted:** 20 October 2017; **Received (in revised form):** 9 December 2017; **Accepted:** 22 December 2017

© The Author(s) 2018. Published by Oxford University Press.

This is an Open Access article distributed under the terms of the Creative Commons Attribution Non-Commercial License (<http://creativecommons.org/licenses/by-nc/4.0/>), which permits non-commercial re-use, distribution, and reproduction in any medium, provided the original work is properly cited. For commercial re-use, please contact [journals.permissions@oup.com](mailto:journals.permissions@oup.com)

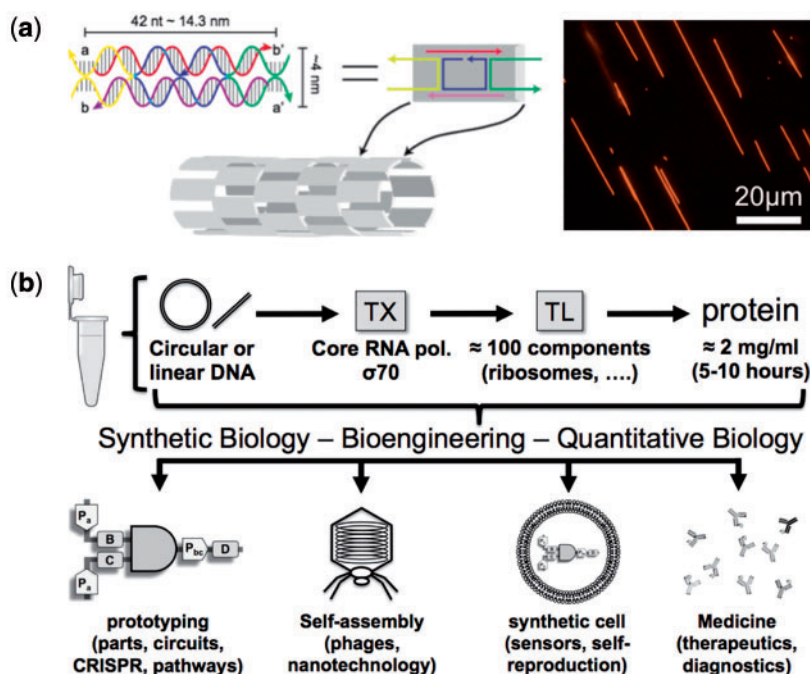


**Figure 1.** (a) DNA nanotubes self-assemble from tiles composed of 5 ssDNA oligomers. Complementary regions on the oligomers bind together to form a DNA tile; at each corner of the DNA tile there is a single-stranded domain (sticky end) serving as programmable binding sites for other tiles. Formation of tubular structures occurs due to the angle at which tiles bind via complementary sticky ends (8) (left). A representative fluorescence microscopy image of DNA nanotubes labeled with Cy 3, in which the nanotubes are in TAE buffer and adhered to the surface of the microscope coverslip for optimal imaging (right). (b) Overview of the all *E. coli* cell-free system used in this work (2).

a few hours in active *E. coli* TXTL. This deficiency renders DNA nanotubes impractical for both synthetic-cell and intracellular applications that require operational viability for timescales exceeding 10 h (1). Previous reports on the stability of DNA origami in cell lysates incorporated sodium dodecyl sulfate (SDS) and deoxycholic acid (DCA), rendering the lysate inactive (10). We found that SDS and DCA inactivate TXTL as well, suppressing GFP expression (Supplementary Figure S1). This suggests that cellular lysates, which include SDS and DCA are not a good model system for a live cytoplasmic environment.

Herein, we explore the utility of modifying oligonucleotide strands to improve the resilience of DNA nanotubes and of modifying the composition of *E. coli* cell-free extract. We were able to increase the lifetime of nanotubes incubated in TXTL to more than 24 h by combining two approaches: inclusion of Chi-containing double-stranded DNA (dsDNA) as a decoy for the complex RecBCD (11) and phosphorothioate (PS) bonding between bases of sticky ends of the tiles. By achieving lifetimes of over 24 h, we approach the ability to integrate tile-based DNA nanotubes with intracellular applications and gene expression systems. Our results suggest that two dominant contributors to degradation of DNA in *E. coli* cell extract are RecBCD and deoxyribonucleases (DNases) (12).

## 2. Materials and methods

### 2.1 TXTL preparation and reactions

The all *E. coli* cell-free TXTL system was prepared using BL21 Rosetta two competent cells from Novagen using procedures described previously (2, 3, 13, 14). Reactions are composed of 33% crude lysate with the remaining 67% being amino acids, salts, an energy buffer and other cofactors. A typical TXTL reaction is composed of 50 mM HEPES pH 8, 1.5 mM ATP and GTP,

0.9 mM CTP and UTP, 0.2 mg/ml tRNA, 0.26 mM coenzyme A, 0.33 mM NAD, 0.75 mM cAMP, 0.068 mM folinic acid, 1 mM spermidine, 30 mM 3-PGA, 2% PEG8000, 10–15 mM maltose or 20–40 mM maltodextrin, 1.5–3 mM of each of the 20 amino acids, 40–120 mM K-glutamate and 2–7 mM Mg-glutamate. Plasmid DNA concentration range from 0 to 2 nM while DNA nanotube concentration was kept at 200 nM. Chi6 dsDNA were used at 0 or 10 μM. The TXTL system used in this work is commercially available from Arbor Biosciences, under the name myTXTL.

### 2.2 Fluorescence anisotropy assays

Anisotropy and deGFP expression experiments were carried out in 2 μl reactions assembled using a Labcyte Echo Liquid Handler 550 in Costar 96 well, V-bottom plates. Kinetic experiments were carried out at 29°C or room temperature in a Biotek Synergy Neo2. To monitor GFP fluorescence, monochromators were set to excitation 485 nm and emission 528 nm. Parallel and perpendicular polarization was measured using a filter cube with an excitation filter of 540 nm and emission filter of 590 nm. The dichroic mirror in the filter cube had a cut-off of 550 nm.

### 2.3 Nanotube assembly

Lyophilized DNA oligonucleotides were purchased from Integrated DNA Technologies (Coralville, IA, USA), resuspended in water, quantitated by UV absorbance at 260 nm using a Thermo Scientific Nanodrop 2000c Spectrophotometer, and stored at –20°C. All samples were stored or mixed using DNA Lo-bind tubes (# 022431021).

Nanotubes were annealed at either 3 or 1.8 μM tile concentration by mixing each tile strand at 3 or 1.8 μM (final concentration), in Tris-Acetate-EDTA (TAE) and 12.4 mM MgCl<sub>2</sub>. Nanopure water was added to achieve the appropriate concentration of

components. All nanotube designs, except those which were to be ligated, were annealed using an Eppendorf Mastercycler PCR machine by heating the sample to 90°C, and cooling it to 25°C over a 6 h period. Nanotubes which were to be ligated were annealed by heating the sample to 90°C, and cooling it to 25°C over a 54 h period.

Nanotubes were ligated at 1.2 μM using New England Biolabs (NEB) T4 DNA Ligase (# M0202S; 20 000 units) at 1.0 units/μl and NEB T4 DNA Ligase buffer (# B0202S, 10×, 10 mM MgCl<sub>2</sub>, 50 mM Tris-HCl, 1 mM ATP, 10 mM DTT, pH 7.5 at 25°C) at 1×. Nanotubes were incubated at room temperature for at least 2 days in ligation solution preceding experiments.

## 2.4 Fluorescence microscopy

Nanotube samples were imaged using an inverted microscope (Nikon Eclipse TI-E) with 60×/1.40 NA oil immersion objectives. Samples containing nanotubes were imaged at 200 nM tile concentration in *E. coli* cell extract with either 0 or 10 μM Chi6 dsDNA (11). Samples were imaged in chambers made using a Bio-Rad frame-seal (# SLF0601; size: 15 × 15 mm, 65 μl) placed on Fisherbrand microscope cover glass (# 12-545E No. 1, thickness = 0.13–0.17 mm; size: 50 × 22 mm); VWR Micro Slides (Plain, Selected, Pre-cleaned, 25 × 75 mm, 1.0 mm thick, # 48300-025) were placed on the frame seal to complete the imaging chamber. Each sample chamber was imaged throughout the duration of the experiments. The fluorescence microscopy image in Figure 1a was prepared as described by Rothmund et al. (8). The sample preparation method described by Rothmund et al. (8) results in images of distinct, individual nanotubes in one focal plane, as the nanotubes are adhered to the surface of the coverslip. In contrast, imaging DNA nanotubes in crowded environments, such as TXTL, results in bundling of nanotubes not seen in non-crowded buffers in which the nanotubes are annealed (Figures 1a and 2a and c) (15). Nanotubes labeled with Cy3 fluorescent molecule were imaged using a Cy3 filter cube (Semrock Brightline—Cy3-404 C-NTE-ZERO). Exposure time was set to 30 ms. Samples for the 29°C experiments were incubated at 29°C on a Nikon Tokai Hit Thermo Plate (# MATS-VAXKW-D).

## 2.5 Gel electrophoresis

Ligated DNA nanotubes were diluted to 180 nM in pure water. To denature the nanotubes, the nanotubes were mixed 1:1 with 8 M urea and then heated to 90°C for 5 min. Denatured nanotube solution was mixed 1:1 with gel loading buffer II (Ambion, AM8547) and loaded into a 1.0 mm 12% polyacrylamide denaturing gel. As a control, we used a 10 base DNA ladder (Invitrogen). Gel electrophoresis was done at 100 V for 90 min, followed by 20 min of gel staining in 1× TBE with 0.2× Syber Gold (Invitrogen, S11494). Imaging was done using a ChemiDoc MP Imaging System (Bio-Rad, Universal Hood III).

## 3. Results and discussions

### 3.1 Nanotubes degrade rapidly within active *E. coli* TXTL

We investigated degradation of DNA nanotubes in the all *E. coli* TXTL system (2) (Figure 1) using fluorescence microscopy and fluorescence anisotropy. Because TXTL includes all the components required for protein synthesis *in vitro* in physiological conditions, other cellular functions such as linear DNA degradation proceed as well due to the remaining cellular machinery present in the lysate. In the *E. coli* TXTL, the major enzyme responsible for linear DNA degradation is the RecBCD enzyme complex (11, 16).

Variants of the tile-based DNA nanotubes degrade within a few hours after addition into TXTL reactions (Figure 2a). We used fluorescence anisotropy to monitor in real time the degradation of nanotubes labeled with Cy3 (Ex/Em 540/590 nm). Fluorescence anisotropy relies on the change in rotational diffusion of molecules. The difference in fluorescence polarization of the parallel and perpendicular intensities is measured and fluorescence anisotropy is calculated as  $r = (I_{\text{parallel}} - I_{\text{perpendicular}}) / (I_{\text{total}})$ . Larger molecules have larger fluorescence anisotropy signals. Consequently, the degradation of DNA nanotubes is observed as a decrease of fluorescence anisotropy. In TAE buffer, i.e. in the absence of degradation, there is no significant change in anisotropy of DNA structures and tiles as long as DNA adsorption is inhibited using a poly-T ssDNA molecule (Supplementary Figure S10). Anisotropy data were fitted using a simple exponential decay model:

$$b_1 - b_2 e^{-t/b_3}$$

The time constant  $b_3$  is reported in Supplementary Table S4 for all variations of nanotubes, temperature and Chi concentration. To quickly assess nanotube robustness in TXTL, we first tested two nanotube variants in which tiles have 8 base-long sticky ends, with and without a single stranded extension (toehold) (Figure 2 and Supplementary Figure S7a). The rapid degradation of the DNA nanotubes observed by fluorescence microscopy was confirmed by fluorescence anisotropy. The decrease in anisotropy begins immediately, suggesting digestion of the DNA nanotubes begins within 5 min of their addition to the extract (Figure 2b). In general, we observe that the anisotropy signal of nanotubes incubated in TXTL decreases reaching a steady-state comparable to that of a control sample of DNA nanotubes incubated with DNase I at room temperature in TAE buffer (Supplementary Figure S10). Nanotubes assembled from tiles without a toehold (8bNT) were slightly more robust than the toehold variant based on microscopy data. The effect was insignificant in anisotropy assays. We hypothesize that the toehold provides an easier access to RecBCD for degradation.

### 3.2 Nanotube tile structure influences degradation rates

Nanotube tile structure, for example sticky end length or inclusion of additional binding sites, can be designed to suit different purposes. To thoroughly characterize degradation of nanotubes with different tile structures in TXTL, we worked with four different tile variants. Increasing the length of the sticky ends results in an increased melting temperature of nanotubes. We considered nanotubes with either 5-base (5b) or 8-base (8b) sticky ends (Supplementary Figures S2 and S3). For each case, we considered an additional tile variant that includes a toehold region on one of the sticky ends (Supplementary Figure S4). The toehold region can be used to link other ligands to the nanotubes (17), or to incorporate strand displacement reactions at the sticky ends (18). We examined degradation of 5b and 8b nanotubes both with (5bT, 8bT) and without (5bNT, 8bNT) toeholds.

Of the four designs studied, the 8b nanotubes outlast the 5b nanotubes at both room temperature and 29°C (Figure 2 and Supplementary Figures S5–S7). At room temperature, 8b nanotubes degrade in under 3 h (Figure 2a), while 5bT and 5bNT nanotubes degrade in under an hour (Supplementary Figure S5a). Degradation occurs more quickly at 29°C, with 8bNT nanotubes degrading within 3 h (Supplementary Figure S7 and

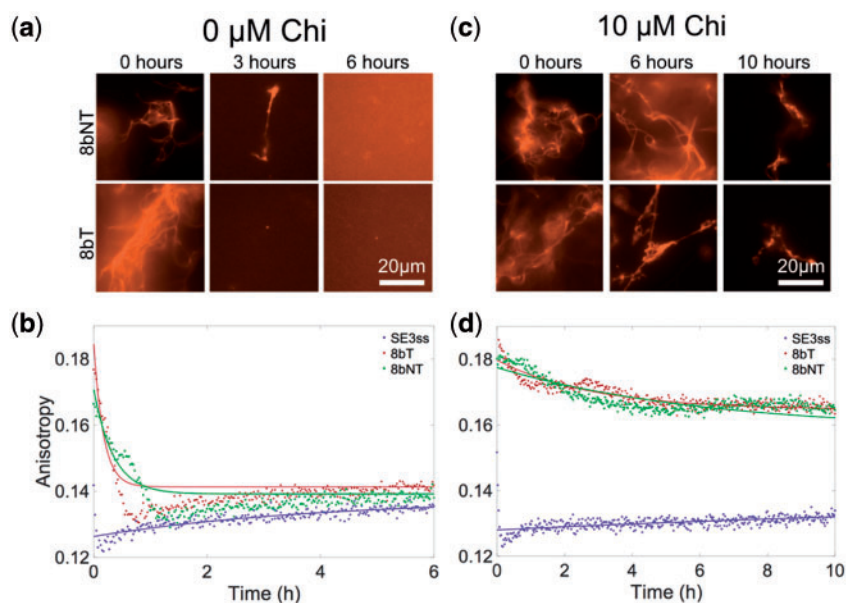


**Figure 2.** Enhancing the stability of DNA nanotubes in TXTL with Chi-site DNA. (a) Fluorescence microscopy kinetics of 8-base DNA nanotubes with (8bT) and without (8bNT) a toehold site incubated in *E. coli* TXTL reactions with no double stranded Chi-site DNA present. Bundling of DNA nanotubes is a result of the crowded TXTL environment. (b) Fluorescence anisotropy kinetics of a single stranded DNA oligo (SE3ss) and 8-base DNA nanotubes with (8bT) and without (8bNT) a toehold site incubated in *E. coli* TXTL reactions with no double stranded Chi-site DNA present. Solid lines represent the prediction of a fitted exponential decay model. (c) Fluorescence microscopy kinetics of 8-base DNA nanotubes with (8bT) and without (8bNT) a toehold site incubated in *E. coli* TXTL reactions with 10  $\mu\text{M}$  of double stranded Chi-site DNA. (d) Fluorescence anisotropy kinetics of single stranded DNA oligo (SE3ss) and 8-base DNA nanotubes with (8bT) and without (8bNT) a toehold site incubated in *E. coli* TXTL reactions with 10  $\mu\text{M}$  of double stranded Chi-site DNA (Chi6). Solid lines are the prediction of a fitted exponential decay model (Supplementary Table S4). All the reactions were incubated at room temperature.

Table S4), and 5bT, 5bNT and 8bT nanotubes degrading in under an hour (Supplementary Figures S6 and S7, Table S4).

### 3.3 Nanotube lifetime increased in presence of Chi and chemical modification of the tiles

We hypothesized that by adding double stranded (ds) DNA molecules containing six repeats of the Chi sequence (5'-GCTGGTGG-3') to TXTL reactions, we would see an increase in DNA nanotube lifetime (11). We recently demonstrated that Chi6 inhibits the degradation of linear dsDNA in TXTL by sequestering RecBCD, with the optimal concentration of Chi6 for protein expression being 2–4  $\mu\text{M}$ . We choose to use 10  $\mu\text{M}$  Chi6 in order to maximize nanotube stability at the cost of slightly depressed protein expression (Supplementary Figure S11).

At room temperature, 8bT and 8bNT nanotubes last up to 10h in the presence of 10  $\mu\text{M}$  Chi6 in the cell-free extract (Figure 2c). Anisotropy assays indicate that the nanotube degradation is not complete, evidenced by the fact that the absolute values of anisotropy for 8bT and 8bNT nanotubes with 10  $\mu\text{M}$  Chi do not converge with those of the 8bT and 8bNT in the absence of Chi (Figure 2d). This suggests that aggregates not visible in microscopy experiments might remain for time periods greater than 10h.

Robustness of nanotubes under different environmental stressors, such as chemical or thermal stress, is improved with ligation (19). Ligation seals the breaks, or nicks, in the sugar-phosphate backbone found at the four corners of inter-tile junctions (Figure 3a). Although the ligation efficiency for the 5' end of strand SE2 was lower than that of the other strands, we verified ligation of all four corner nicks via denaturing gel (Supplementary Figure S12). Both the microscopy images (Figure 3b, Supplementary Figure S8), and the time constants obtained from the fluorescence anisotropy observations (Figure 3c) suggest that ligation enhances nanotube

robustness in TXTL (Supplementary Table S4). Increasing the ligation efficiency could lead to even greater improvement in the resilience of the DNA nanotubes in TXTL.

Nucleases, such as DNase I, are inhibited by PS bonded DNA. PS bonds connect the sugar-phosphate backbone of one base to another, much as a phosphodiester bond does in native DNA, with sulfur replacing the native oxygen (Supplementary Figure S4b). Exonucleases are inhibited by PS bonds located at the ends of DNA, while endonucleases are inhibited by incorporating PS bonds into the entire backbone of a DNA structure (20).

Because the 8bNT nanotube design is the most stable in TXTL, we designed 8bNT tiles with PS bonds between the 8 bases of the sticky ends of the tiles (Figure 3d). By modifying the sticky ends, we expected to impede nanotube degradation by RecBCD and other exonucleases. The lifetimes of PS bonded DNA nanotubes was more than double that of unmodified 8bNT nanotubes, as observed by fluorescence microscopy and fluorescence anisotropy (Figure 3e and f). At room temperature, 8bPS tubes lasted up to 10h without the Chi6 DNA, with aggregates of degraded tubes visible at 10h. In the presence of the Chi6 DNA, at room temperature, 8bPS nanotubes remained at least 24h in TXTL. At 29°C, 8bPS nanotubes degraded in under 3h without the Chi6 DNA and between 3 and 6h with the Chi6 DNA (Supplementary Figure S9).

## 4. Summary and conclusions

DNA nanotubes are rapidly degraded in the TXTL environment. Incorporating Chi DNA into the cell-free system extends the lifetime of the DNA nanotubes, confirming the previous observations that RecBCD is the major actor responsible for degradation (11). Modifications to the DNA tiles themselves also affect the lifetime of the DNA nanotubes. Lengthening the tile sticky

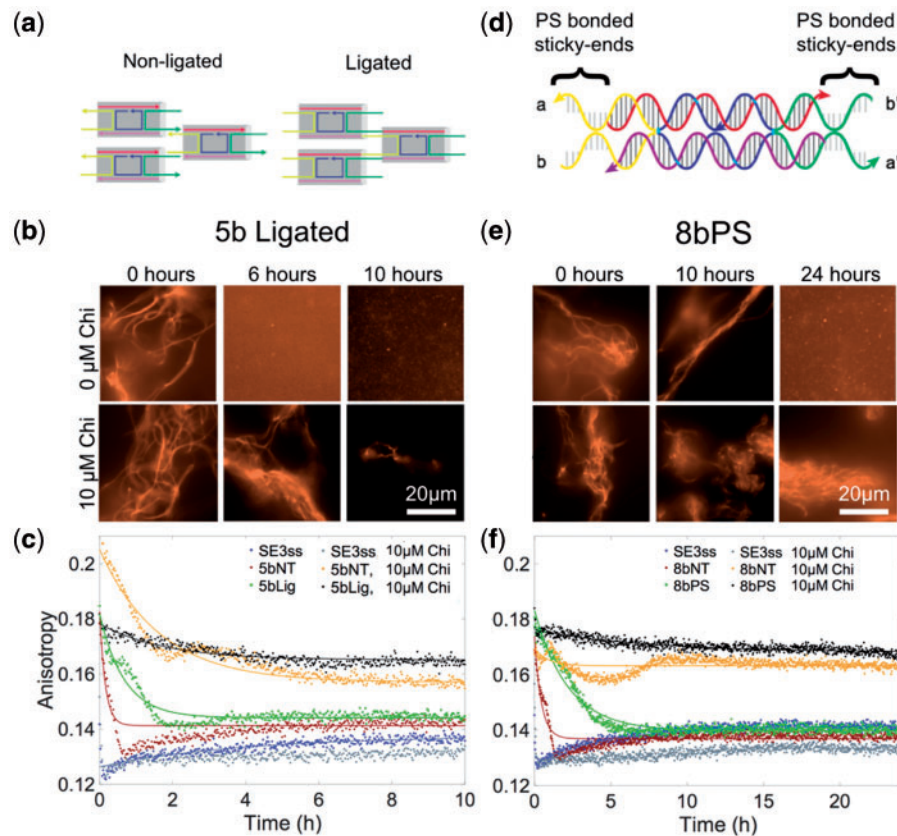


**Figure 3.** Enhancing the stability of DNA nanotubes in TXTL systems with Chi-site DNA and chemical modifications (ligation or phosphorothioate bonding of sticky ends). (a) Cartoon of ligation. (b) Fluorescence microscopy kinetics of 5-base DNA nanotubes with a ligation of the sticky ends of the tiles incubated in *E. coli* TXTL reactions with and without Chi-site DNA present. (c) Fluorescence anisotropy kinetics, and exponential decay model prediction (solid lines), of a single stranded DNA oligo (SE3ss) and 5-base DNA nanotubes with (5bNT) and without (5bLig) a ligation of the sticky ends of the tiles incubated in *E. coli* TXTL reactions with and without Chi-site DNA present. (d) Cartoon of phosphorothioation. (e) Fluorescence microscopy kinetics of 8-base DNA nanotubes with phosphorothioate bonded sticky ends of the tiles incubated in *E. coli* TXTL reactions with and without Chi-site DNA present. (f) Fluorescence anisotropy kinetics of a single stranded DNA oligo (SE3ss) and 8-base DNA nanotubes with (PSE) and without (8bNT) the phosphorothioation of the sticky ends of the tiles incubated in *E. coli* TXTL reactions with and without Chi-site DNA present. The predictions of our exponential decay model are shown as solid lines (Supplementary Table S4). All the reactions were incubated at room temperature.

ends increases nanotube stability, and eliminating toehold overhangs increases the lifetime even further. PS bonding on the sticky ends of the nanotubes was the most effective tile modification, while ligating these same domains had a small effect.

This study is limited to DNA nanotubes and does not consider what the chemical modifications to the cell-free extract or to the DNA self-assembling components may have on other DNA structures, such as DNA origami (7) or crystals (21). We conjecture that more tightly packed assemblies such as origami might be stable for several days with appropriate chemical modifications. It is unclear if other modifications to the extract could be used to prevent other nucleases from acting on DNA in the cytoplasmic environment as Chi DNA was used to specifically target RecBCD. Chi DNA is specific to RecBCD so it would not extend DNA nanotube lifetimes in cytoplasmic environments other than *E. coli*. However, in these cases we expect that it would still be possible to mitigate nanotube degradation by introducing or up-regulating the concentration of competitive binding sites for the corresponding enzymes.

While DNA nanostructures have a variety of potential applications in biological contexts, the stability of these structures has not been previously thoroughly demonstrated in cell-like environments mimicking cytoplasmic conditions. Many DNA structures are designed with the intention for intracellular use,

as scaffolding, drug delivery or synthetic cell components, making the absence of characterization of these structures in cell-like environments a considerable impediment to these aims.

We demonstrated that TXTL can be used as an experimental platform to test the robustness of DNA nanostructures and to engineer new ones with longer lifetimes in cytoplasmic environment. This method could be used as a testbed to rapidly prototype robust DNA nanostructures for *in vivo* applications.

## Supplementary data

Supplementary Data are available at SYNBO Online.

## Acknowledgements

We thank PWK Rothmund for discussions about DNA nanotubes.

## Funding

U.S. Department of Energy under Award Number [DE-SC0010595 to EF], which paid for reagents and supplies used at UC Riverside; the Human Frontier Science Program [RGP0037/2015 to V.N.].

**Conflict of interest:** Noireaux laboratory receives research funds from Arbor Biosciences, a distributor of myTXTL cell-free protein expression kit.

## References

- Chen, Y.J., Groves, B., Muscat, R.A. and Seelig, G. (2015) DNA nanotechnology from the test tube to the cell. *Nat. Nanotechnol.*, 10, 748–760.
- Garamella, J., Marshall, R., Rustad, M. and Noireaux, V. (2016). The all *E. coli* TX-TL toolbox 2.0: a platform for cell-free synthetic biology. *ACS Synth. Biol.*, 5, 344–355.
- Shin, J. and Noireaux, V. (2012) An *E. coli* cell-free expression toolbox: application to synthetic gene circuits and artificial cells. *ACS Synth. Biol.*, 1, 29–41.
- Douglas, S.M., Bachelet, I. and Church, G.M. (2012) A logic-gated nanorobot for targeted transport of molecular payloads. *Science*, 335, 831–834.
- Langecker, M., Arnaut, V., Martin, T.G., List, J., Renner, S., Mayer, M., Dietz, H. and Simmel, F.C. (2012) Synthetic lipid membrane channels formed by designed DNA nanostructures. *Science*, 338, 932–936.
- Park, S.H., Yin, P., Liu, Y., Reif, J.H., LaBean, T.H. and Yan, H. (2005) Programmable DNA self-assemblies for nanoscale organization of ligands and proteins. *Nano Lett.*, 5, 729–733.
- Rothemund, P.W. (2006) Folding DNA to create nanoscale shapes and patterns. *Nature*, 440, 297–302.
- , Ekani-Nkodo, A., Papadakis, N., Kumar, A., Fygenson, D.K. and Winfree, E. (2004) Design and characterization of programmable DNA nanotubes. *J. Am. Chem. Soc.*, 126, 16344–16352.
- Winfree, E., Liu, F., Wenzler, L.A. and Seeman, N.C. (1998) Design and self-assembly of two-dimensional DNA crystals. *Nature*, 394, 539–544.
- Mei, Q., Wei, X., Su, F., Liu, Y., Youngbull, C., Johnson, R., Lindsay, S., Yan, H. and Meldrum, D. (2011) Stability of DNA origami nanoarrays in cell lysate. *Nano Lett.*, 11, 1477–1482.
- Marshall, R., Maxwell, C.S., Collins, S.P., Beisel, C.L. and Noireaux, V. (2017) Short DNA containing chi sites enhances DNA stability and gene expression in *E. coli* cell-free transcription-translation systems. *Biotechnol. Bioeng.*, 114, 2137–2141.
- Sitaraman, K., Esposito, D., Klarmann, G., Le Grice, S.F., Hartley, J.L. and Chatterjee, D.K. (2004) A novel cell-free protein synthesis system. *J. Biotechnol.*, 110, 257–263.
- Shin, J. and Noireaux, V. (2010). Efficient cell-free expression with the endogenous *E. coli* RNA polymerase and sigma factor 70. *J. Biol. Eng.*, 4, 8.
- Sun, Z.Z., Hayes, C.A., Shin, J., Caschera, F., Murray, R.M. and Noireaux, V. (2013) Protocols for implementing an *Escherichia coli* based TX-TL cell-free expression system for synthetic biology. *J. Vis. Exp.*, e50762.
- Glaser, M., Schnauß, J., Tschirner, T., Schmidt, B.S., Moebius-Winkler, M., Käs, J.A. and Smith, D.M. (2016) Self-assembly of hierarchically ordered structures in DNA nanotube systems. *New J. Phys.*, 18, 055001.
- Sun, Z.Z., Yeung, E., Hayes, C.A., Noireaux, V. and Murray, R.M. (2014) Linear DNA for rapid prototyping of synthetic biological circuits in an *Escherichia coli* based TX-TL cell-free system. *ACS Synth. Biol.*, 3, 387–397.
- Sharma, J., Chhabra, R., Cheng, A., Brownell, J., Liu, Y. and Yan, H. (2009) Control of self-assembly of DNA tubules through integration of gold nanoparticles. *Science*, 323, 112–116.
- Zhang, D.Y. and Seelig, G. (2011) Dynamic DNA nanotechnology using strand-displacement reactions. *Nat. Chem.*, 3, 103–113.
- O'Neill, P., Rothemund, P.W., Kumar, A. and Fygenson, D.K. (2006) Sturdier DNA nanotubes via ligation. *Nano Lett.*, 6, 1379–1383.
- Stein, C.A., Subasinghe, C., Shinozuka, K. and Cohen, J.S. (1988) Physicochemical properties of phosphorothioate oligodeoxynucleotides. *Nucleic Acids Res.*, 16, 3209–3221.
- Hao, Y., Kristiansen, M., Sha, R., Birktoft, J.J., Hernandez, C., Mao, C. and Seeman, N.C. (2017) A device that operates within a self-assembled 3D DNA crystal. *Nat. Chem.*, 9, 824–827.

# Engineering DNA nanotubes for resilience in an *E. coli* TXTL system

Melissa A. Klocke<sup>1†</sup>, Jonathan Garamella<sup>2†</sup>, Hari K. K. Subramanian<sup>1</sup>, Vincent Noireaux<sup>2\*</sup> and Elisa Franco<sup>1\*</sup>

<sup>1</sup>Mechanical Engineering, University of California, Riverside, Riverside, CA, 92521, USA

<sup>2</sup>School of Physics and Astronomy, University of Minnesota, Minneapolis, MN, 55455, USA

†These authors contributed equally to this work.

\*Corresponding authors, E-mails: [efranco@engr.ucr.edu](mailto:efranco@engr.ucr.edu), [noireaux@umn.edu](mailto:noireaux@umn.edu)

## Content:

Item	Title	Pages
Table S1	Sequences for the tiles with 5-base long sticky ends and their variants	3
Table S2	Sequences for the tiles with 8-base long sticky ends and their variants	5
Table S3	Sequences for the Chi6 dsDNA	7
Table S4	Time constants for DNA nanotubes degrading in TXTL	9
Figure S1	Test of SDS and DCA on protein synthesis	2
Figure S2	Schematics of tile variants with 5-base sticky ends	4
Figure S3	Schematics of tile variants with 8-base sticky ends	6
Figure S4	DNA nanotube structures with variants and chemical modifications	8
Figure S5	5-base DNA nanotubes in TXTL systems with chi-site DNA at room temperature	10
Figure S6	5-base DNA nanotubes in TXTL systems with chi-site DNA at 29°C	11
Figure S7	8-base DNA nanotubes in TXTL systems with chi-site DNA at 29°C	12
Figure S8	Ligated DNA nanotubes in TXTL systems at 29°C	13
Figure S9	DNA nanotubes with phosphorothioate (PS) bonded sticky-ends in TXTL systems at 29°C	14
Figure S10	Effect of thymine repeating DNA oligonucleotide and DNase1 on DNA nanotubes in TAE buffer	15
Figure S11	Effect of deGFP production on DNA nanotube degradation	16
Figure S12	Ligation efficiency of DNA nanotubes	17

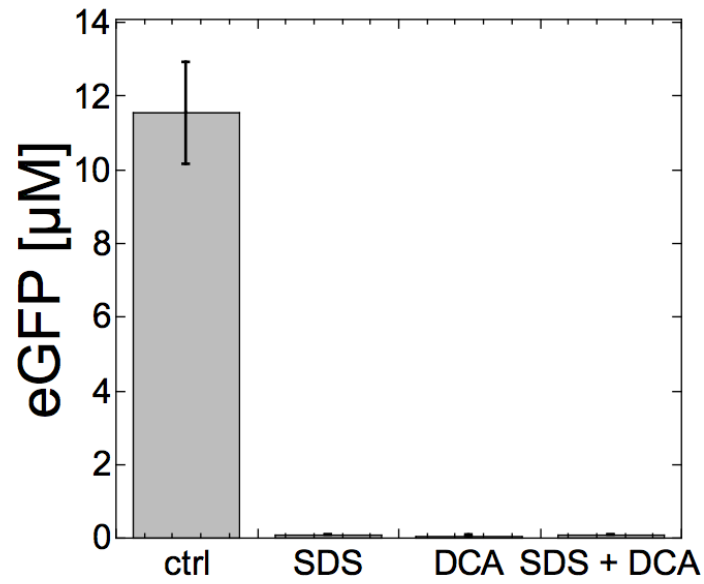


**Figure S1.** The effect of SDS and DCA on TXTL protein synthesis. 1 nM P70a-deGFP plasmid was added to a standard TXTL reaction. The reaction was split into four identical aliquots, to which was either added water (ctrl), sodium dodecyl sulfate (SDS) (0.1% volume final) and/or deoxycholic acid (DCA) (0.1% volume final). The SDS and DCA percentages are the same as in (Mei et al., 2011). The reactions were incubated at 29°C for 12 hrs. Error bars represent standard deviation from 3 repeats.

## DNA Sequences

Oligonucleotides were purchased from Integrated DNA Technologies (Coralville, IA, USA). Sequences for 5-base SE1, SE2 NoTH, SE3 Cy3, SE4, and SE5, are taken from (Rothmund et al., 2004). DNA sequences for SE2 TH and all 8-base strands are taken from (Green et al., submitted, 2017). Modified DNA sequences for ligation were taken from (O'Neill et al., 2006). Modified DNA sequences for PS bonded sticky-end strands we designed by the authors. DNA sequences for Chi6 dsDNA are taken from (Marshall et al., 2017).

Name	Sequence
SE1	5' - CTC AGT GGA CAG CCG TTC TGG AGC GTT GGA CGA AAC T
SE1 NT 5'P	5' - /5Phos/CTC AGT GGA CAG CCG TTC TGG AGC GTT GGA CGA AAC T
SE2 NT	5' - GTC TGG TAG AGC ACC ACT GAG AGG TA
SE2 T	5' - <b>TGG TAT</b> TGT CTG GTA GAG CAC CAC TGA GAG GTA
SE2 NT 5'P	5' - /5Phos/GTC TGG TAG AGC ACC ACT GAG AGG TA
SE2 NS	5' - GT AGA GCA CCA CTG AG
SE3 CY3	5' - T Cy3/CCA GAA CGG CTG TGG CTA AAC AGT AAC CGA AGC ACC AAC GCT
SE4	5' - CAG ACA GTT TCG TGG TCA TCG TAC CT
SE4 5'P	5' - /5Phos/CAG ACA GTT TCG TGG TCA TCG TAC CT
SE5	5' - CGA TGA CCT GCT TCG GTT ACT GTT TAG CCT GCT CTA C
SE5 NT 5'P	5' - /5Phos/CGA TGA CCT GCT TCG GTT ACT GTT TAG CCT GCT CTA C

**Table S1.** Sequences for the tiles with 5-base long sticky ends and their variants. Bold sequences indicate toehold domains. An added phosphate on the 5' end of ssDNA strands is indicated by /5Phos/.

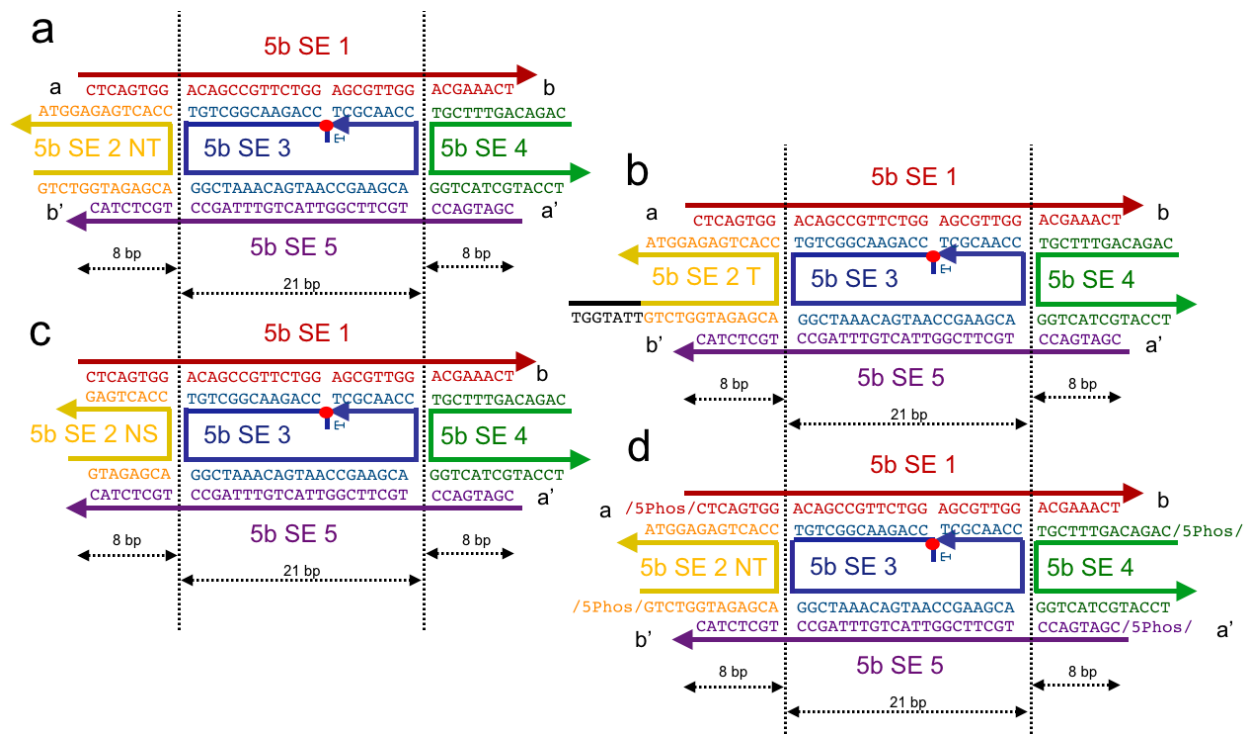


**Figure S2.** Tile variants with 5-base sticky ends. The red dot on each tile represents the Cy3 label. **(a)** Tile with 5-base sticky ends and no toehold domain. **(b)** Tile with 5-base sticky ends and 7-base long toehold domain. **(c)** Tile with 5-base sticky ends on SE4 and no sticky ends on SE2, which assemble into DNA tile monomers rather than nanotubes. **(d)** Tile with 5-base sticky ends and an additional phosphate on the 5' ends of SE1, SE2, SE4, SE5 for ligation.

Name	Sequence
8b SE1	5' - AGT GGA CAG CCG TTC TGG AGC GTT GGA CGA AAC T
8b SE2 NT	5' - TCG TGC CCG AGC ACC ACT GAG AGG TA
8b SE2 T	5' - <b>TGT AAT ATC</b> GTG CCC GAG CAC CAC TGA GAG GTA
8b SE2 PS	5' - T*C*G *T*G*C *C*C*G AGC ACC ACT *G*A*G *A*G*G *T*A
8b SE3 Cy3	5' - T Cy3/CCA GAA CGG CTG TGG CTA AAC AGT AAC CGA AGC ACC AAC GCT
8b SE4	5' - GGG CAC GAA GTT TCG TGG TCA TCG TAC CTC TC
8b SE4 PS	5' - G*G*G *C*A*C *G*A*A GTT TCG TGG TCA TCG *T*A*C *C*T*C *T*C
8b SE5	5' - CGA TGA CCT GCT TCG GTT ACT GTT TAG CCT GCT C

**Table S2.** Sequences for the tiles with 8-base long sticky ends and their variants. Bold sequences indicate toehold domains. Phosphorothioate bonds between bases designated with an asterisk.

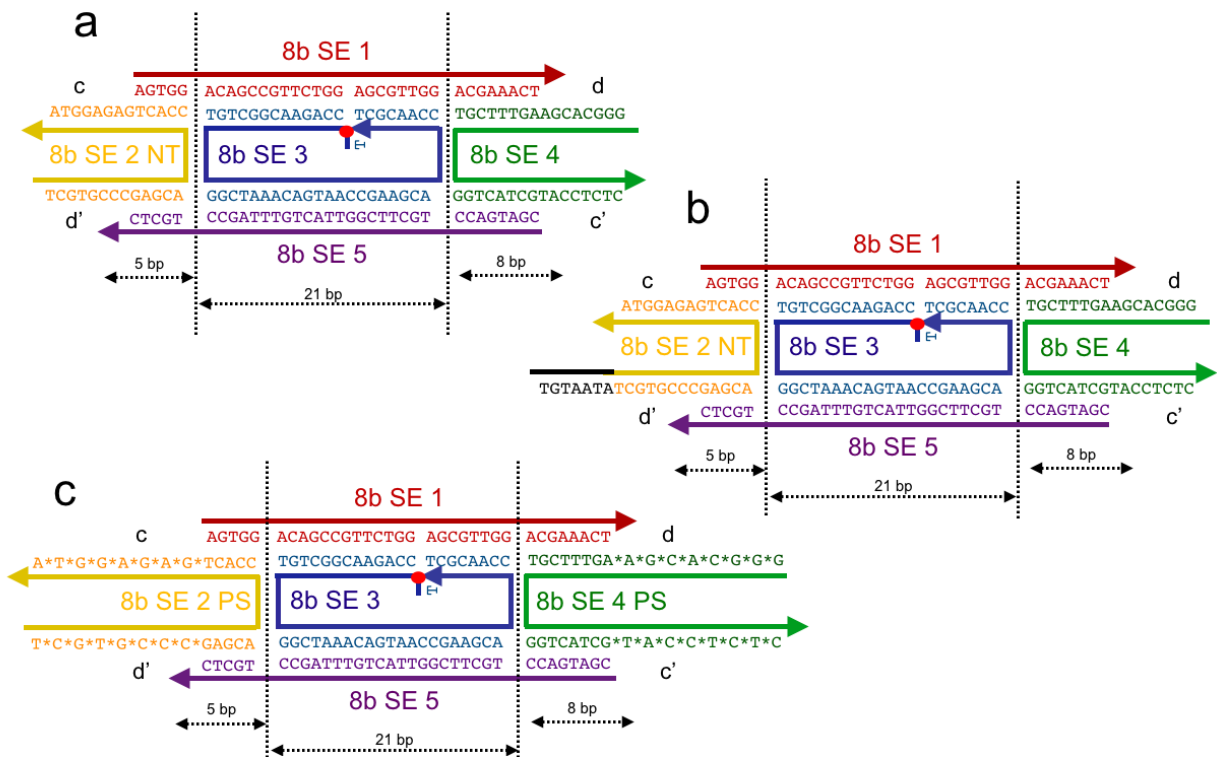


**Figure S3.** Tile variants with 8-base sticky ends. The red dot on each tile represents the Cy3 label. **(a)** Tile with 8-base sticky ends and no toehold domain. **(b)** Tile with 8-base sticky ends and 7-base long toehold domain. **(c)** Tile with 8-base sticky ends with Phosphorothioate bonds between the bases on the sticky ends of 8b SE2 and 8b SE4.

Name	Sequence
Chi6.fwd	5' - TCA CTT CAC TGC TGG TGG CCA CTG CTG GTG GCC ACT GCT GGT GGC CAC TGC TGG TGG CCA CTG CTG GTG GCC ACT GCT GGT GGC CA
Chi6.rev	5' - TGG CCA CCA GCA GTG GCC ACC AGC AGT GGC CAC CAG CAG TGG CCA CCA GCA GTG GCC ACC AGC AGT GGC CAC CAG CAG TGA AGT GA

**Table S3.** Sequences for the Chi6 dsDNA.

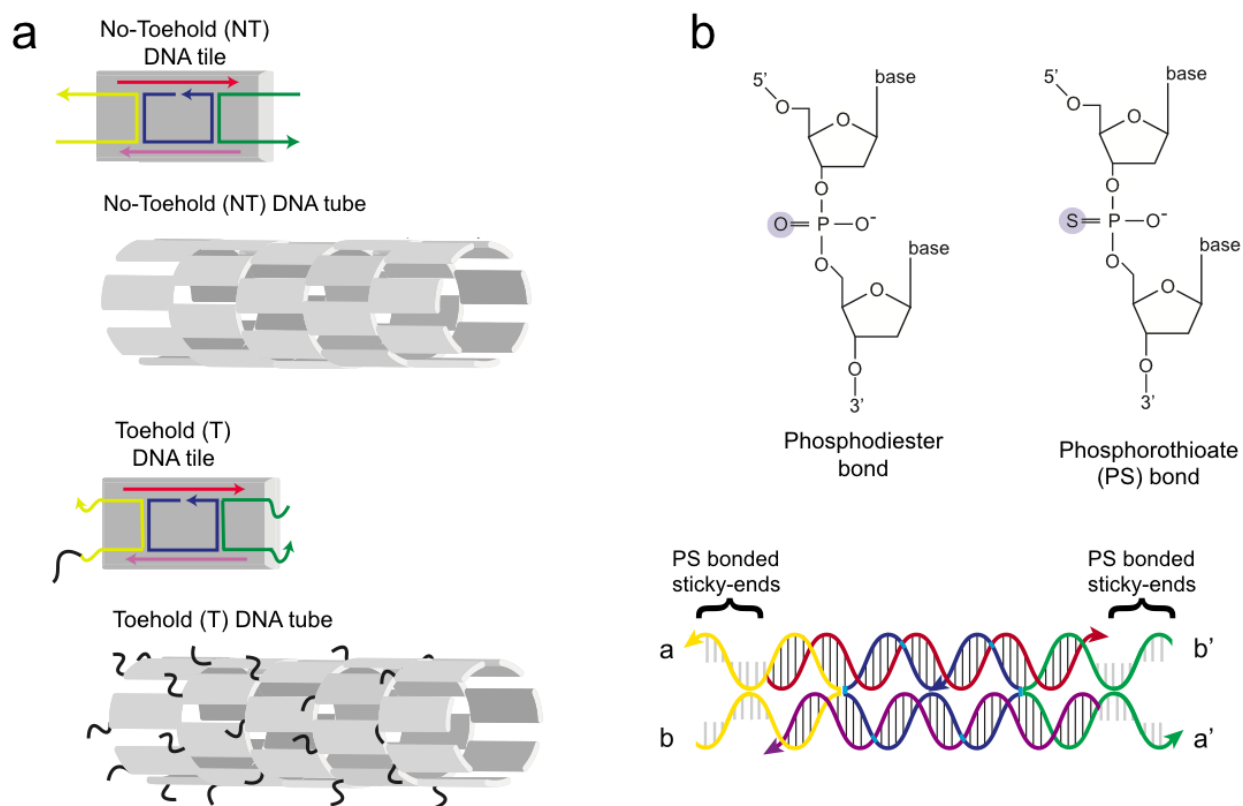


**Figure S4.** DNA nanotube structures with variants and chemical modifications. **(a)** Cartoon of DNA tile and nanotube without toehold domain (top) and with toehold domain (bottom). **(b)** Chemical structure of a phosphorothioate (PS) bond versus a phosphodiester bond and (top) the location of PS bonds on the DNA nanotubes (bottom).

### Data fitting

Fluorescence anisotropy data were fitted using a simple model of exponential decay:

$$b_1 - b_2 e^{-t/b_3}$$

The model was fitted to data using MATLAB's `nlinfit` function using custom scripts. Throughout the paper the model prediction is overlapped to each data set as a solid line having the same color as the data. The fitted time constants  $b_3$  obtained for the data sets are reported in Table S4.

Name	0 $\mu\text{M}$ Chi		10 $\mu\text{M}$ Chi	
	23C	29°C	23C	29°C
5bT	10.3	10.2	188.2	98.45
5bNT	18.0	9.3	193.3	255.6
8bT	10.3	11.6	170.7	174.4
8bNT	20.78	17.5	370.7	414.3
5bLig	<b>40.7</b>	<b>20.6</b>	<b>107.0</b>	<b>344.8</b>
8bPS	130.8	24.9	436.4	144.9

**Table S4.** Fitted time constants (minutes) obtained from anisotropy experiments for DNA nanotubes incubated in TXTL at room temperature and 29°C in the presence and absence of 10  $\mu\text{M}$  Chi.

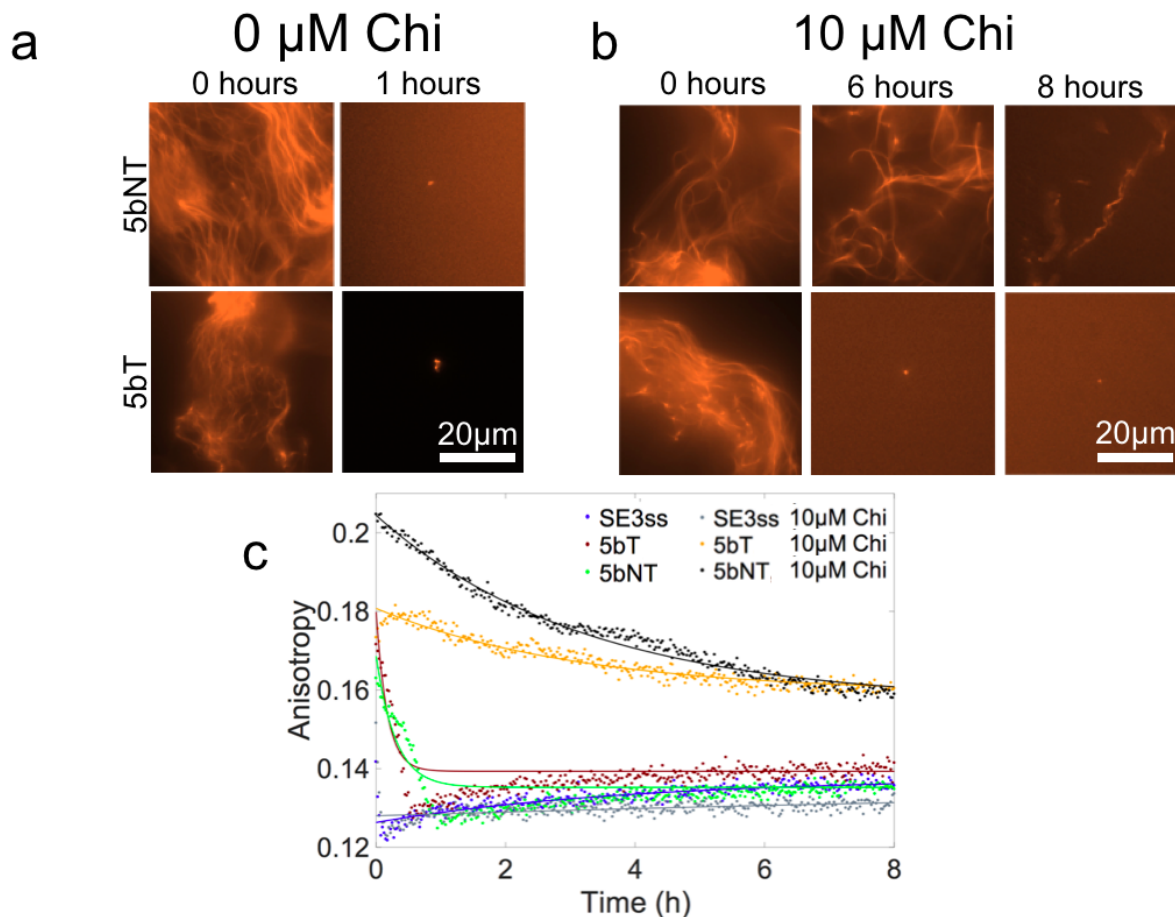


**Figure S5.** Enhancing the stability of 5-base DNA nanotubes in TXTL systems with chi-site DNA at room temperature. **(a)** Fluorescence microscopy kinetics of 5-base DNA nanotubes with (5bT) and without (5bNT) a toehold domain incubated in *E. coli* TXTL reactions without double stranded chi-site DNA present. **(b)** Fluorescence microscopy kinetics of 5-base DNA nanotubes with (5bT) and without (5bNT) a toehold site incubated in *E. coli* TXTL reactions with double stranded chi-site DNA present. **(c)** Fluorescence anisotropy kinetics of a single stranded DNA oligo (SE3ss) and 5-base DNA nanotubes with (5bT) and without (5bNT) a toehold site incubated in *E. coli* TXTL reactions with and without double stranded chi-site DNA present. Solid lines represent the prediction of our fitted exponential decay model.

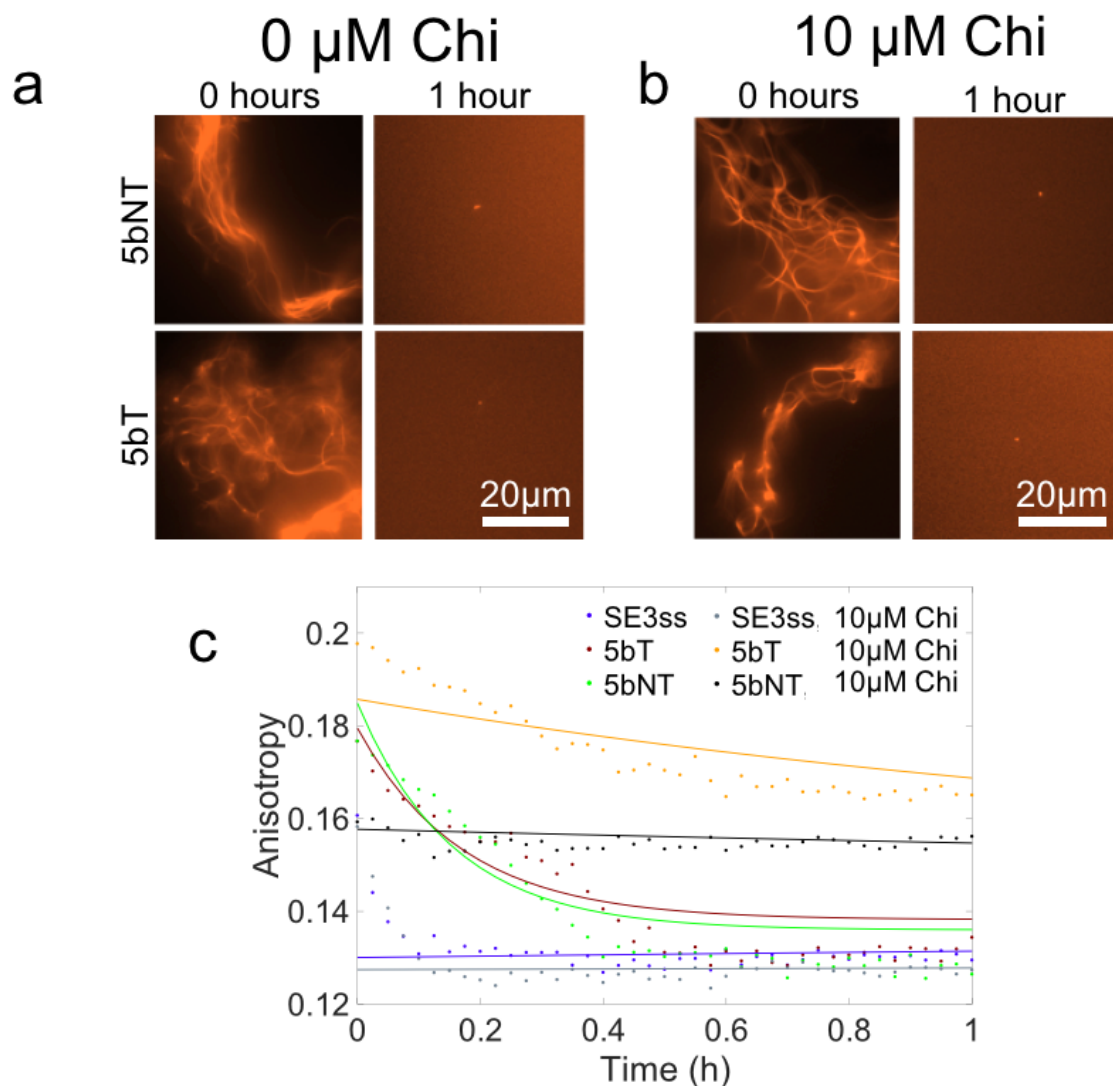


**Figure S6.** Enhancing the stability of 5-base DNA nanotubes in TXTL systems with chi-site DNA at 29°C. **(a)** Fluorescence microscopy kinetics of 5-base DNA nanotubes with (5bT) and without (5bNT) a toehold site incubated in *E. coli* TXTL reactions without double stranded chi-site DNA present. **(b)** Fluorescence microscopy kinetics of 5-base DNA nanotubes with (5bT) and without (5bNT) a toehold site incubated in *E. coli* TXTL reactions with double stranded chi-site DNA present. **(c)** Fluorescence anisotropy kinetics of a single stranded DNA oligo (SE3ss) and 5-base DNA nanotubes with (5bT) and without (5bNT) a toehold site incubated in *E. coli* TXTL reactions with and without double stranded chi-site DNA present. Solid lines represent the prediction of our fitted exponential decay model.

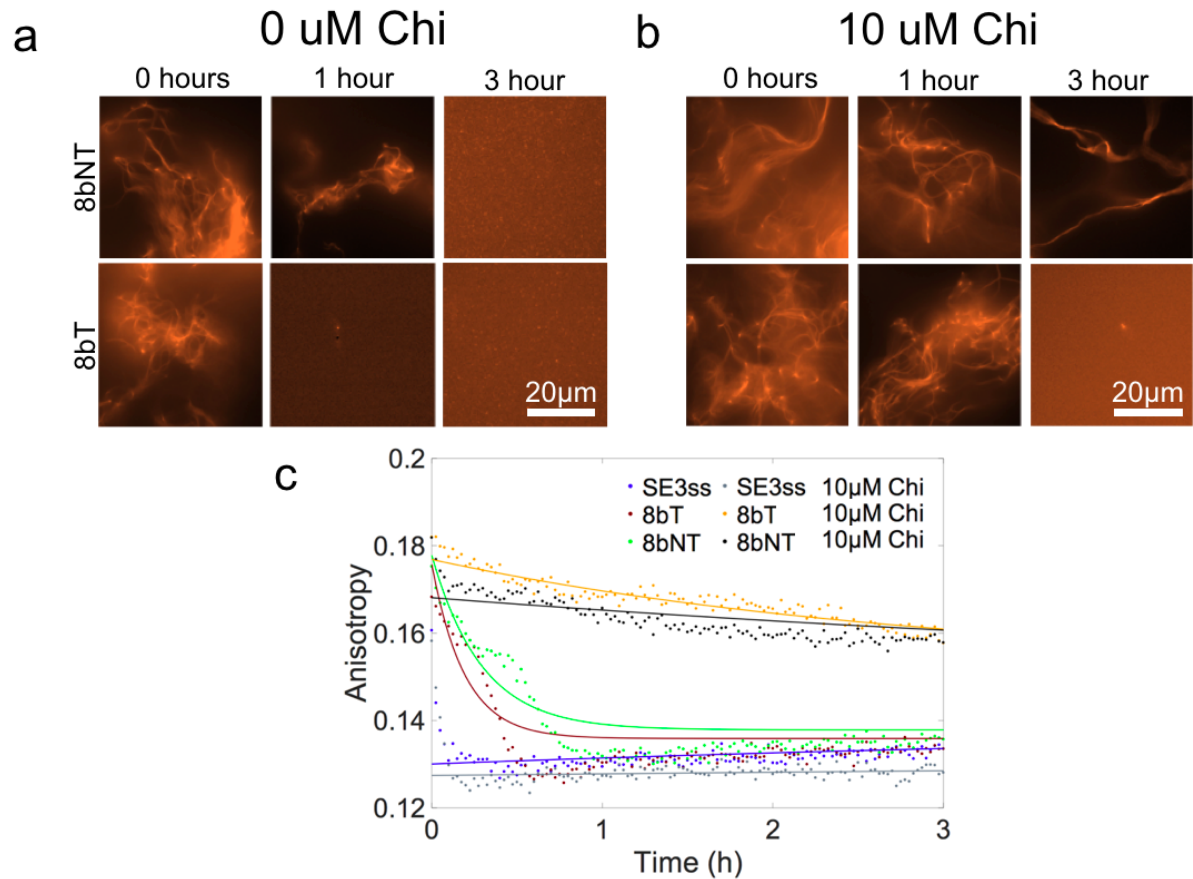


**Figure S7.** Enhancing the stability of 8-base DNA nanotubes in TXTL systems with chi-site DNA at 29°C. **(a)** Fluorescence microscopy kinetics of 8-base DNA nanotubes with (8bT) and without (8bNT) a toehold site incubated in *E. coli* TXTL reactions without double stranded chi-site DNA present. **(b)** Fluorescence microscopy kinetics of 8-base DNA nanotubes with (8bT) and without (8bNT) a toehold site incubated in *E. coli* TXTL reactions with double stranded chi-site DNA present. **(c)** Fluorescence anisotropy kinetics of a single stranded DNA oligo (SE3ss) and 8-base DNA nanotubes with (8bT) and without (8bNT) a toehold site incubated in *E. coli* TXTL reactions with and without double stranded chi-site DNA present. Solid lines represent the prediction of our fitted exponential decay model.

## 5b Ligated

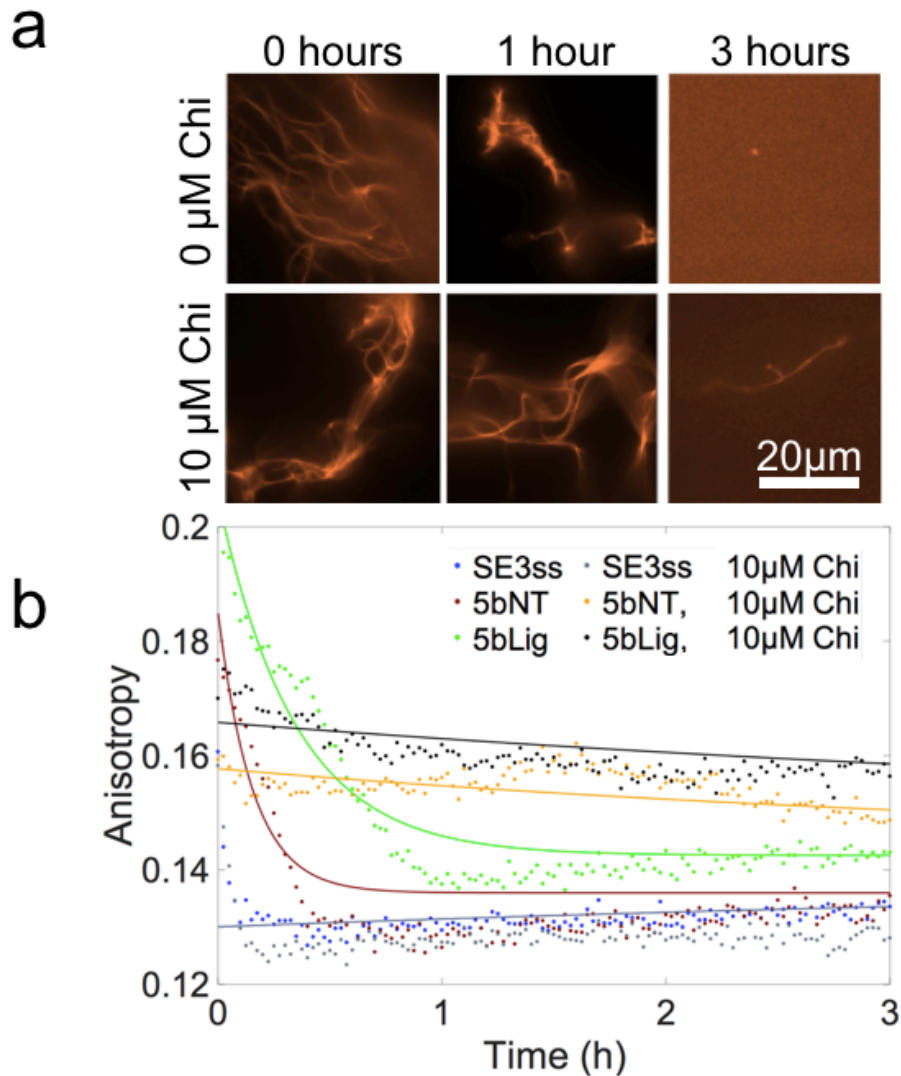


**Figure S8.** The effect of DNA nanotube ligation on stability in TXTL systems at 29°C. **(a)** Fluorescence microscopy kinetics of 5bLig nanotubes in the presence or absence of Chi-site DNA. **(b)** Fluorescence anisotropy kinetics of a single stranded DNA oligo (SE3ss) and 5-base DNA nanotubes with (5bLig) and without (5bNT) modification via ligation incubated in *E. coli* TXTL reactions with and without double stranded chi-site DNA present. Solid lines represent the prediction of our fitted exponential decay model.

# 8bPS

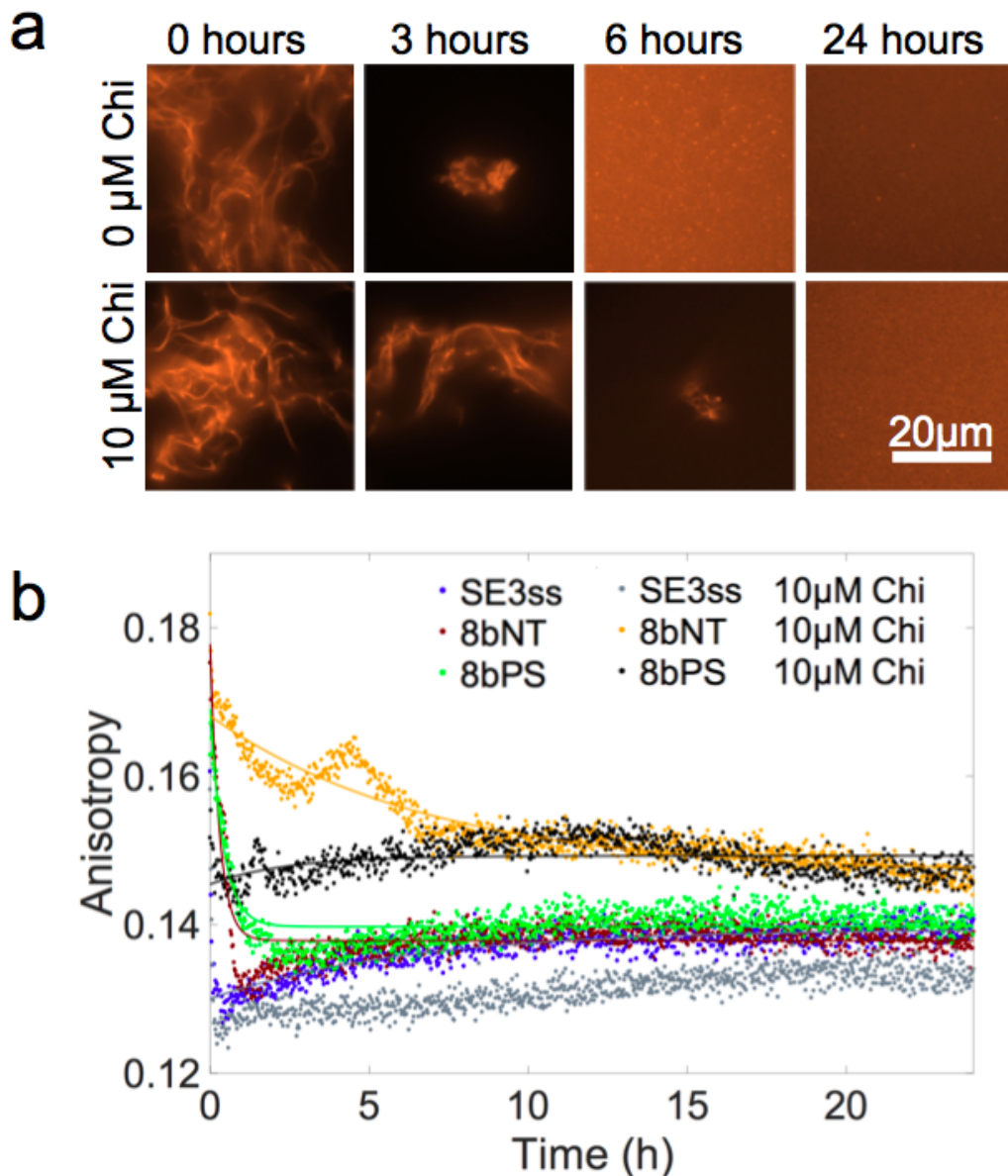


**Figure S9.** The effect of phosphorothioate (PS) bonded sticky-ends of DNA nanotubes on stability in TXTL systems at 29°C. **(a)** Fluorescence microscopy kinetics of 8bPS nanotubes in the presence or absence of Chi-site DNA. **(b)** Fluorescence anisotropy kinetics of a single stranded DNA oligo (SE3ss) and 8-base DNA nanotubes with (8bPS) and without (8bNT) modification via phosphorothioate bonded sticky ends incubated in *E. coli* TXTL reactions with and without double stranded chi-site DNA present. Solid lines represent the prediction of our fitted exponential decay model.

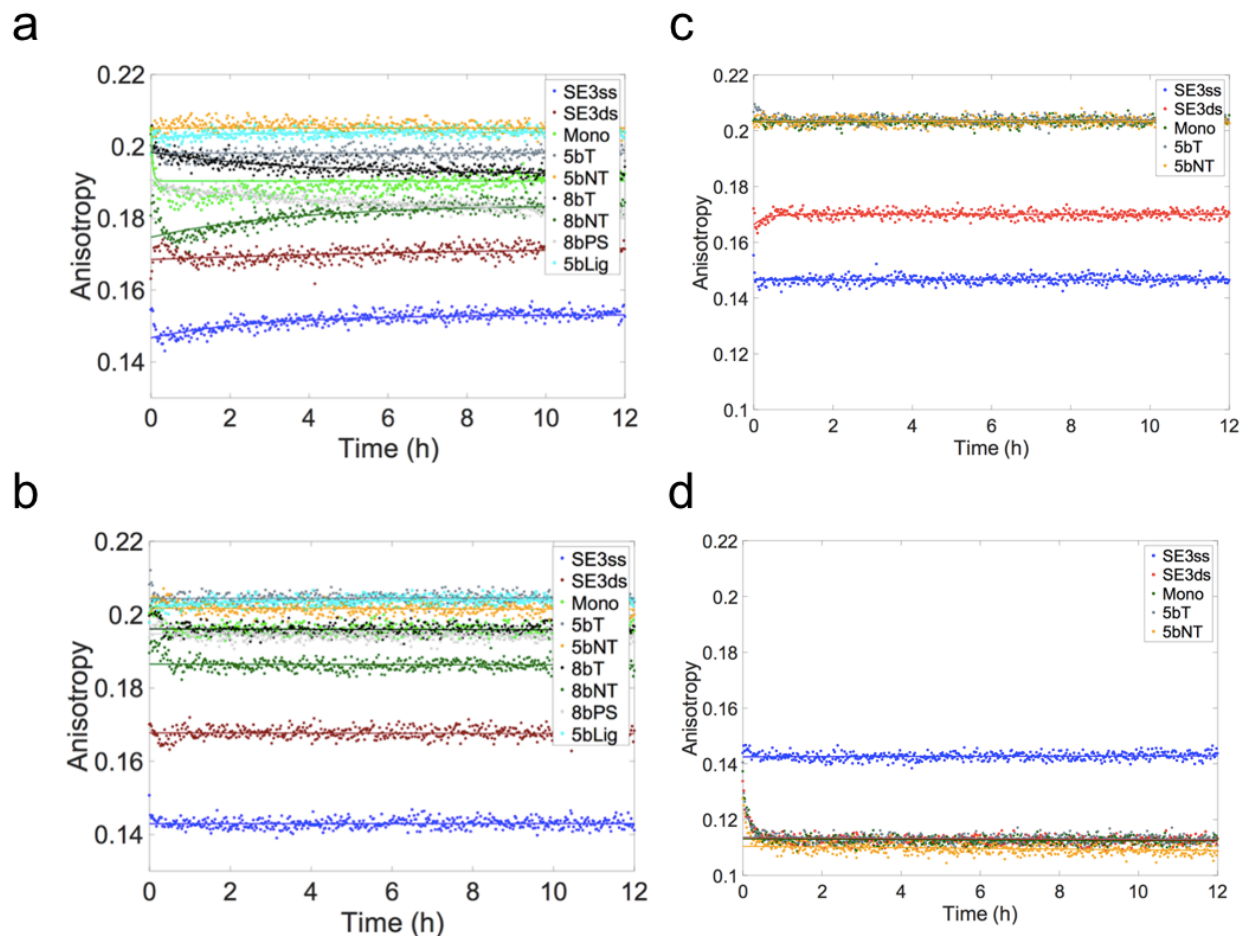


**Figure S10.** Fluorescence anisotropy kinetics in TAE buffer at room temperature. Solid lines represent the prediction of our fitted exponential decay model. **(a)** Fluorescence anisotropy kinetics of all nanotubes studied in this work incubated in TAE buffer at room temperature. **(b)** Fluorescence anisotropy kinetics of all nanotubes studied in this work incubated in TAE buffer at room temperature with  $2 \mu\text{M}$  5' - TTTTTTTTT - 3' oligonucleotide acting as an adsorption prohibitor. Addition of poly-T (thymine) ssDNA oligonucleotide reduces adsorption of DNA on the sample walls and stabilizes anisotropy signals. **(c)** Fluorescence anisotropy kinetics of nanotube controls, 5bT, and 5bNT nanotubes incubated in TAE buffer with  $2 \mu\text{M}$  5' - TTTTTTTTT - 3' oligonucleotide and no DNase 1. **(d)** Fluorescence anisotropy kinetics of nanotube controls, 5bT, and 5bNT nanotubes incubated in TAE buffer with  $2 \mu\text{M}$  5' - TTTTTTTTT - 3' oligonucleotide and 10% vol. DNase 1.

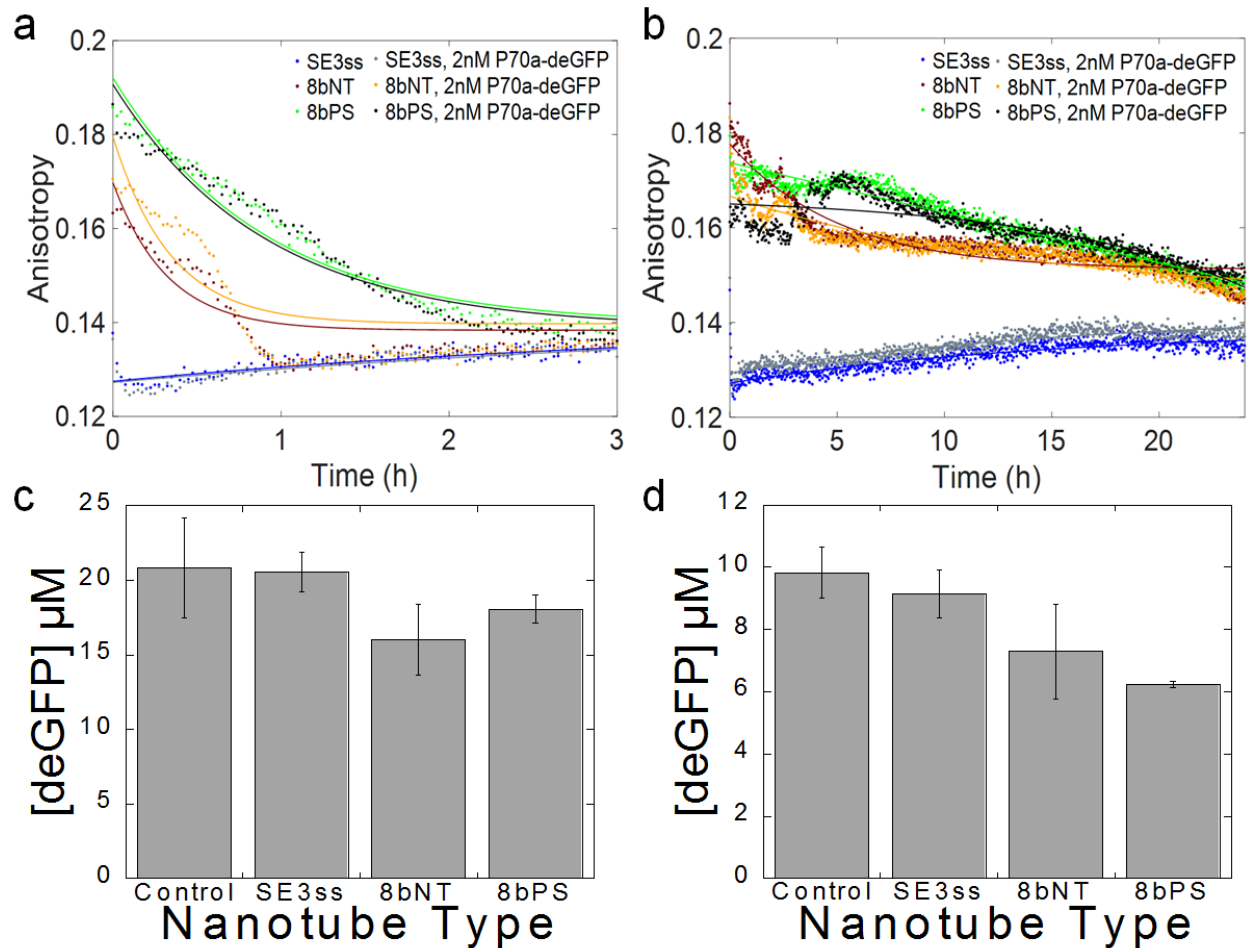


**Figure S11.** Effect of protein expression on DNA nanotube degradation at 29°C and vice versa. (a) Fluorescence anisotropy kinetics of 8bNT and 8bPS nanotubes in the presence or absence of P70a-deGFP using 0  $\mu\text{M}$  Chi. (b) Fluorescence anisotropy kinetics of 8bNT and 8bPS nanotubes in the presence or absence of P70a-deGFP using 10  $\mu\text{M}$  Chi. Solid lines represent the prediction of our fitted exponential decay model. (c) The effect of DNA nanotubes on protein synthesis with 2 nM P70a-deGFP and 0  $\mu\text{M}$  Chi. [deGFP] was measured after 12 hours incubation at 29°C with 200nM DNA nanotubes. Control indicates the absence of DNA nanotubes. (d) The effect of DNA nanotubes on protein synthesis with 2 nM P70a-deGFP and 10  $\mu\text{M}$  Chi. Control indicates the absence of DNA nanotubes.

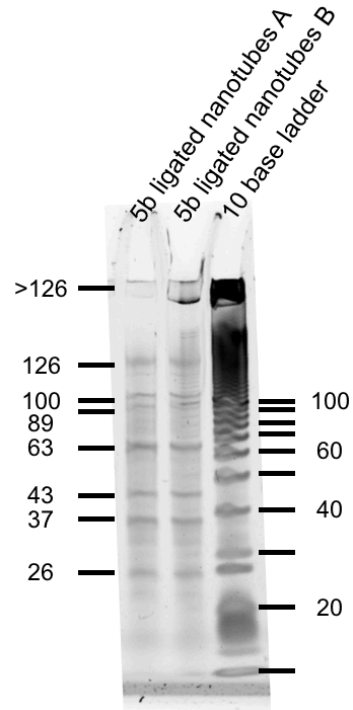


**Figure S12.** A representative denaturing polyacrylamide gel demonstrating the ligation efficiency of DNA nanotubes. The left and middle lanes contain strands from the 5b ligated nanotube, while the right lane contains a ten base ladder. The strands in the left lane, 5b ligated nanotubes A, were annealed in a 1X TAE, 12.5 mM MgCl<sub>2</sub> buffer. The strands in the middle lane, 5b ligated nanotubes B, were annealed in a buffer composed of 10 mM MgCl<sub>2</sub>, 10 mM DTT, 30 mM tris-HCl and 1 mM ATP as described in O'Neill *et al.*, 2006. Both the left and middle lanes contain a distribution of bands indicating the presence of ligated products of different length; this suggests that while each of the 4 tile nicks has a 5' phosphate to enable ligation, the ligation process is not completely efficient. The 26, 37 and 43 base-long products are non-ligated SE2 and SE4, SE1 and SE5, and SE3 strands, respectively. The 63 base-long products correspond to 1-nick ligated SE1/SE2, SE2/SE5, SE5/SE4, or SE4/SE1 strands. The 89 base-long products correspond to the 2-nick ligated products of SE2/SE5/SE4 or SE4/SE1/SE5, while the 100 base-long products correspond to ligation of SE1/SE2/SE5 or SE5/SE4/SE1. The product of 3-nick ligation, SE5/SE4/SE1/SE2, is 126 bases long. When all 4 nicks are ligated, a loop is formed that corresponds to a band above the 126 base band. While the efficiency of the ligation of all 4 nicks has room for improvement, these results are comparable to that of O'Neill *et al.* The intensity of bands corresponding to longer ligation products increased as the time nanotubes were incubated in the ligation solution increased. DNA nanotube in TXTL experiments were carried out with nanotubes annealed in the 1X TAE, 12.5 mM MgCl<sub>2</sub> buffer as the ligation of the SE2/SE1 nick was more efficient than in nanotubes annealed in the buffer composed of 10 mM MgCl<sub>2</sub>, 10 mM DTT, 30 mM tris-HCl and 1 mM ATP. More efficient ligation may further improve the stability of DNA nanotubes in TXTL.

## References

Green, L.N.; Subramanian, H.K.K.; Mardanlou, V.; Kim, J.; Hariadi, R.F.; Franco, E. Autonomous dynamic control of DNA nanostructure self-assembly. Submitted, 2017. Downloadable at: <https://tinyurl.com/y82oug87>

Marshall, R., Maxwell, C.S., Collins, S.P., Beisel, C.L., and Noireaux, V. (2017). Short DNA containing chi sites enhances DNA stability and gene expression in E. coli cell-free transcription-translation systems. *Biotechnol Bioeng* *114*, 2137-2141.

Mei, Q., Wei, X., Su, F., Liu, Y., Youngbull, C., Johnson, R., Lindsay, S., Yan, H., and Meldrum, D. (2011). Stability of DNA origami nanoarrays in cell lysate. *Nano Lett* *11*, 1477-1482.

O'Neill, P., Rothmund, P.W., Kumar, A., and Fygenson, D.K. (2006). Sturdier DNA nanotubes via ligation. *Nano Lett* *6*, 1379-1383.

Rothmund, P.W., Ekani-Nkodo, A., Papadakis, N., Kumar, A., Fygenson, D.K., and Winfree, E. (2004). Design and characterization of programmable DNA nanotubes. *J Am Chem Soc* *126*, 16344-16352.